Elastic $\bar{p}d$ scattering and total $\bar{p}d$ cross sections

Yu. N. Uzikov[1,2] and J. Haidenbauer[3,4]
[1]*Laboratory of Nuclear Problems, Joint Institute for Nuclear Research, 141980 Dubna, Russia*
[2]*Physics Department, Moscow State University, 119991 Moscow, Russia*
[3]*Institute for Advanced Simulation, Forschungszentrum Jülich, D-52425 Jülich, Germany*
[4]*Institut für Kernphysik and Jülich Center for Hadron Physics, Forschungszentrum Jülich, D-52425 Jülich, Germany*
(Received 12 December 2012; revised manuscript received 19 April 2013; published 20 May 2013)

Elastic $\bar{p}d$ scattering is studied within the Glauber theory based on the single- and double $\bar{p}N$ scattering mechanisms. The full spin dependence of the elementary $\bar{p}N$ scattering amplitudes is taken into account and both the S- and D-wave components of the deuteron are considered. The treatment of the spin dependence is done in a (properly modified) formalism developed recently by Platonova and Kukulin for the $pd \to pd$ scattering process. Predictions for differential cross sections and the spin observables A_y^d, $A_y^{\bar{p}}$, A_{xx}, A_{yy} are presented for antiproton beam energies between 50 and 300 MeV, using amplitudes generated from the $\bar{N}N$ interaction model developed by the Jülich group. Total polarized cross sections are calculated utilizing the optical theorem. The efficiency of the polarization buildup for antiprotons in a storage ring is investigated.

DOI: 10.1103/PhysRevC.87.054003 PACS number(s): 25.10.+s, 25.40.Qa, 25.45.−z

I. INTRODUCTION

The present investigation is motivated by the plans of the PAX Collaboration [1] to measure the transversity of the proton (antiproton) in double-polarized Drell-Yang processes at an upgrade of the FAIR facility in Darmstadt. In order to achieve this aim an intense polarized beam of antiprotons is required. A possibility to overcome the experimental challenge to obtain such a polarized beam is seen in scattering of antiprotons off a polarized ^{1}H target in rings [2]. Analogous experiments performed for the proton case by the FILTEX Collaboration [3] at 23 MeV and a recent COSY study where protons were scattering off a polarized hydrogen at 49 MeV [4] showed that indeed a polarized (proton) beam can be achieved via the so-called spin-filtering effect, i.e. by exploiting the fact that via the scattering process protons are removed (lost) from the ring at different rates for different initial polarization states [3]. According to theoretical interpretations [5] of the data [3,4], the polarization buildup effect appears solely due to the hadronic interaction of the incoming proton with the target.

Whereas the spin dependence of the nucleon-nucleon (NN) interaction is very well known at the considered energies, which allows one to calculate reliably the spin-filtering effect for protons, there is practically no corresponding information for the antiproton-nucleon ($\bar{N}N$) interaction. For this reason a test experiment for the spin-filtering effect in the antiproton-hydrogen interaction is planned at the AD ring at the CERN facility [6,7].

In view of the unknown spin dependence of the $\bar{p}N$ interaction, the interaction of antiprotons with a polarized deuteron is also of interest for the issue of the antiproton polarization buildup. This option was discussed in a previous paper by us [8]. In that work the single-scattering approximation was used for the calculation of the polarized total $\bar{p}d$ cross sections for energies in the region 50–300 MeV. The spin dependence of the elementary $\bar{p}N$ amplitudes was taken into account in this approximation only in collinear kinematics using the $\bar{N}N$ interaction model of the Jülich group [9–12]. The $\bar{p}N$ double-scattering effects were only accounted for in the computation of the *unpolarized* total and differential cross sections, and were found to be in the order of 10%–15% [8]. Spin observables for $\bar{p}d$ elastic scattering and shadowing effects (double scattering) in polarized total cross sections were not considered in that work. A calculation of such observables, including double-scattering effects, is the main aim of the present work. Indeed corresponding results are certainly desirable, specifically in view of the prospect that a discrimination of existing models of the $\bar{p}N$ interaction could be feasible on the basis of a comparison with expected data [7]. Antiproton polarization buildup in the context of $\bar{p}d$ scattering was also studied in a recent work by Salnikov [13], utilizing the results from the Nijmegen $\bar{p}p$ partial wave analysis [14] from 1994. (Note that an updated partial wave analysis has been presented recently by Zhou and Timmermans [15].)

In the present paper we consider elastic $\bar{p}d$ scattering within the Glauber theory of multistep scattering [16–18], taking into account the full spin dependence of the elementary $\bar{p}N$ scattering amplitudes. There are several studies of the accuracy of the Glauber theory in the literature [19–24] which demonstrate that corrections to the eikonal approximation, which is the basis of this theory, are small in the region of intermediate energies about $\sim$1 GeV. The reliability of the Glauber approach at intermediate energies was studied recently in Ref. [25] via a comparison with rigorous Faddeev calculations for the case of identical spinless bosons interacting by means of a simple Malfliet-Tjon interaction potential. The results of Ref. [25] for such a "bosonic" nd system show that even at rather low energies, 100–200 MeV, the difference between the Faddeev and the Glauber calculations is just about 10%–15% for the total cross section. Rather good agreement was found also for the differential cross section in the forward hemisphere, excluding the region of the diffraction minimum [25].

For antiproton-nucleus scattering the Glauber theory can be applied at lower energies [26,27] as compared to the proton-nucleus reaction. The amplitude for elastic scattering

of antiprotons off nuclei is strongly peaked in the forward direction due to strong annihilation effects in the $\bar{p}N$ interaction, supporting the applicability of the eikonal approximation (see Ref. [8] and reference therein). In the present work the S- and D-wave components of the deuteron and both the single and double $\bar{p}N$ scattering mechanisms are taken into account. The treatment of the spin dependence is based on a proper modification of the formalism developed recently by Platonova and Kukulin [28,29] for pd elastic scattering. In their papers the formalism was successfully applied for describing spin observables of the $pd \to pd$ process at 250–1000 MeV. An independent confirmation of the findings of [28] was reported recently by us [30].

The spin dependence of the $\bar{p}d \to \bar{p}d$ amplitude is very similar to that for $pd \to pd$ scattering, except for the contribution of the charge-exchange channel $\bar{p}p \leftrightarrow \bar{n}n$ which, however, can be taken into account straightforwardly. In the present work we consider the differential cross section and the spin observables A_y^d, $A_y^{\bar{p}}$, A_{xx}, A_{yy} for the $\bar{p}d \to \bar{p}d$ process. Those observables are evaluated here for antiproton beam energies from 50 to 300 MeV employing $\bar{p}N$ amplitudes generated from the Jülich $\bar{N}N$ model [11]. The total polarized cross sections σ_1, σ_2, and σ_3 are calculated on the basis of the optical theorem. We also investigate the efficiency of the polarization buildup for antiprotons in a storage ring. Here Coulomb effects are taken into account within the formalism described in Ref. [8].

The paper is structured in the following way: In Sec. II we introduce briefly the used formalism. In particular, we point out the differences that occur between its application to the pd- and to the $\bar{p}d$ systems. In Sect. III results for $\bar{p}d$ scattering are presented. First we discuss the issue of the applicability of the Glauber theory. Specifically, we assess the angular range for which differential observables can be reliably calculated within this approach. Then predictions for the differential cross section and the spin observables A_y^d, $A_y^{\bar{p}}$, A_{xx}, A_{yy} are given based on elementary $\bar{p}N$ amplitudes taken from the Jülich $\bar{N}N$ models A and D. Finally, our results for the total $\bar{p}d$ cross section are provided, including those for the polarized case. We also provide predictions for the polarization degree of the antiproton beam which is the decisive quantity for the spin-filtering method. The paper ends with a short summary. Relations between amplitudes and considered observables are given in The Appendix.

II. ELEMENTS OF THE FORMALISM FOR $\bar{p}d \to \bar{p}d$ SCATTERING

For the $\bar{p}d \to \bar{p}d$ process we use the formalism developed in Ref. [28] for the process $pd \to pd$, taking into account the specific differences that arise for the $\bar{p}d$ collision. Within the Glauber theory [18] the scattering matrix for elastic $\bar{p}d$ scattering is given by the following matrix element:

$$M_{\bar{p}d}(\mathbf{q}) = \langle f|\hat{M}(\mathbf{q},\mathbf{s})|i\rangle, \tag{1}$$

evaluated between definite initial $|i\rangle$ and final $|f\rangle$ states of the $\bar{p}d$ system. Here $\mathbf{q}$ is the momentum transferred from the initial to the final deuteron in the $\bar{p}d$ collision and $\mathbf{s}$ is the impact parameter of the projectile. In Eq. (1) and in the following we suppress the dependence of $M_{\bar{p}d}$ on the total energy to simplify the notation. The transition operator $\hat{M}$ can be written as

$$\begin{aligned}\hat{M}(\mathbf{q},\mathbf{s}) &= \exp\left(\frac{1}{2}i\mathbf{q}\cdot\mathbf{s}\right)M_{\bar{p}p}(\mathbf{q}) + \exp\left(-\frac{1}{2}i\mathbf{q}\cdot\mathbf{s}\right)M_{\bar{p}n}(\mathbf{q}) \\ &\quad + \frac{i}{2\pi^{3/2}}\int \exp(i\mathbf{q}'\cdot\mathbf{s})[M_{\bar{p}p}(\mathbf{q}_1)M_{\bar{p}n}(\mathbf{q}_2) \\ &\quad + M_{\bar{p}n}(\mathbf{q}_1)M_{\bar{p}p}(\mathbf{q}_2) - M_{\bar{p}p\to\bar{n}n}(\mathbf{q}_1)M_{\bar{n}n\to\bar{p}p}(\mathbf{q}_2)]d^2\mathbf{q}'.\end{aligned} \tag{2}$$

Here $M_{\bar{p}N}(\mathbf{q})$ $(N = p, n)$ is the $\bar{p}N$ scattering matrix, $M_{\bar{p}p\to\bar{n}n}$ $(M_{\bar{n}n\to\bar{p}p})$ is the scattering matrix of the charge-exchange process $\bar{p}p \to \bar{n}n$ $(\bar{n}n \to \bar{p}p)$, and $\mathbf{q}_1 = \mathbf{q}/2 - \mathbf{q}'$ and $\mathbf{q}_2 = \mathbf{q}/2 + \mathbf{q}'$ are the transferred momenta in the first and second $\bar{p}N$ collisions, respectively, in the double-scattering terms. The first two plane-wave terms correspond to the single-scattering mechanism, while the three terms in the integral represent the double-scattering mechanism. These transitions correspond to the diagrams depicted in Fig. 1. It is assumed in Eq. (2) that the deuteron wave function in the matrix element of this operator does not contain the isospin part explicitly. Therefore the last term in Eq. (2) appears with a negative sign coming from the product of the isospin factors at the dpn vertices.

The elementary scattering matrix for elastic $\bar{p}N$ scattering is given by the following expression:

$$\begin{aligned}M_{\bar{p}N} &= A_N + (C_N\boldsymbol{\sigma}_1 + C'_N\boldsymbol{\sigma}_2)\cdot\hat{\mathbf{n}} + B_N(\boldsymbol{\sigma}_1\cdot\hat{\mathbf{k}})(\boldsymbol{\sigma}_2\cdot\hat{\mathbf{k}}) \\ &\quad + (G_N - H_N)(\boldsymbol{\sigma}_1\cdot\hat{\mathbf{n}})(\boldsymbol{\sigma}_2\cdot\hat{\mathbf{n}}) \\ &\quad + (G_N + H_N)(\boldsymbol{\sigma}_1\cdot\hat{\mathbf{q}})(\boldsymbol{\sigma}_2\cdot\hat{\mathbf{q}}).\end{aligned} \tag{3}$$

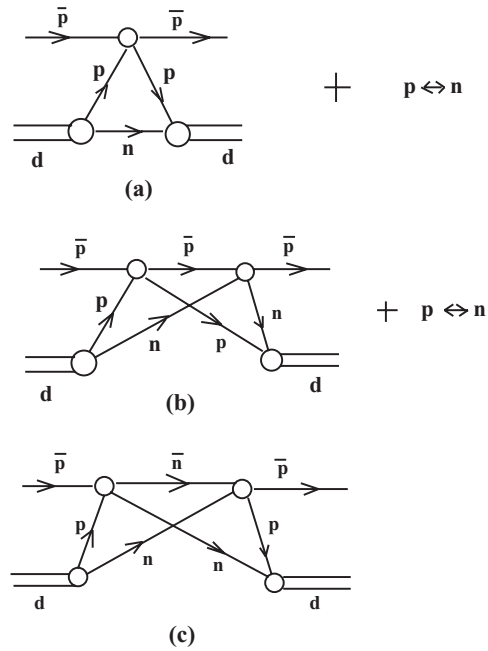

FIG. 1. Mechanisms for $\bar{p}d$ elastic scattering: single scattering (a), double scattering (b), and charge exchange (c).

Here $\boldsymbol{\sigma}_1$ ($\boldsymbol{\sigma}_2$) is the Pauli matrix acting on the spin of the $\bar{p}$ (N) states, $N = p, n$. The unit vectors are defined by $\hat{\mathbf{k}} = (\mathbf{k}_i + \mathbf{k}_f)/|\mathbf{k}_i + \mathbf{k}_f|$, $\hat{\mathbf{q}} = (\mathbf{k}_i - \mathbf{k}_f)/|\mathbf{k}_i - \mathbf{k}_f|$, and $\hat{\mathbf{n}} = [\hat{\mathbf{k}} \times \hat{\mathbf{q}}]$, where $\mathbf{k}_i$ ($\mathbf{k}_f$) denotes the momentum of the incident (outgoing) antiproton. The one for charge-exchange, $M_{\bar{p}p\leftrightarrow\bar{n}n}$, has the same spin structure as given in Eq. (3). We denote the corresponding amplitudes on the right-hand side of Eq. (3) by A_c, C_c, etc. in the following for simplicity reasons.

The amplitudes in Eqs. (1)–(3) are normalized as in Ref. [28] and related to the corresponding differential cross sections via

$$\frac{d\sigma}{dt} = \frac{1}{6} tr M_{\bar{p}d} M^{+}_{\bar{p}d}, \tag{4}$$

$$\frac{d\sigma}{dt} = \frac{1}{4} tr M_{\bar{p}N} M^{+}_{\bar{p}N}, \tag{5}$$

where $t = -\mathbf{q}^2$ is the squared four-momentum transfer in the $\bar{p}d$ or $\bar{p}N$ systems, respectively. The factor in front of the integral in Eq. (2) differs from that in the original Glauber theory [18] due to a different normalization of the invariant scattering matrices M used in Eqs. (1)–(5).

In general, there are 36 transitions in the $\bar{p}d \to \bar{p}d$ process for the different spin states. When accounting for rotational invariance and invariance under parity- and time-reversal transformations, the number of transition matrix elements for the $\bar{p}d \to \bar{p}d$ process reduces to twelve independent complex amplitudes A_i ($i = 1, \ldots, 12$), which can be introduced in the same way as for the $pd \to pd$ process [8,28] (see also the Appendix). The amplitudes A_i can be written in the form

$$A_i(q) = A_i^{(s)}(q) + \frac{i}{2\pi^{3/2}} \int d^2q' \left(A_i^{(d)}(\mathbf{q}, \mathbf{q}') - A_i^{(c)}(\mathbf{q}, \mathbf{q}') \right). \tag{6}$$

Here we introduced the scalar amplitudes for single scattering [Fig. 1(a)], $A_i^{(s)}(q)$, double scattering [Fig. 1(b)], $A_i^{(d)}(\mathbf{q}, \mathbf{q}')$, and double-scattering involving charge exchange [Fig. 1(c)], $A_i^{(c)}(\mathbf{q}, \mathbf{q}')$, using the same notations as in Ref. [28].

The amplitudes $A_i^{(s,d,c)}$ can be expressed via the elastic form factors of the deuteron corresponding to the transitions $S \to S$, $S \to D$, $D \to S$, $D \to D$, from the initial to the final deuteron state, and the elementary amplitudes of $\bar{p}N$ scattering. The explicit expressions can be found in Ref. [28] in the Appendices A and B and, therefore, we refrain from reproducing those lengthy formulas here. Specifically, the formulas for the single-scattering mechanism $A_i^{(s)}$ [Fig. 1(a)] are the same as those for the $pd \to pd$ processs given in Ref. [28] in Table I with the replacement of the elementary amplitudes of pN elastic scattering by the corresponding ones for $\bar{p}N$. However, the integral in Eq. (6), accounting for the double-scattering mechanisms differs from that in Eq. (A.1) in Ref. [28] by two aspects. First, the term $A_i^{(d)}$ in Ref. [28] has an additional factor 2. Second, the permutations $n \leftrightarrow p$ are taken into account here for $A_i^{(s)}(q)$ and $A_i^{(d)}(\mathbf{q}, \mathbf{q}')$, as in Ref. [28], but they do not apply for $A_i^{(c)}(\mathbf{q}, \mathbf{q}')$.

In order to explain the reason for these two differences between the $\bar{p}d \to \bar{p}d$ and $pd \to pd$ amplitudes, let us discuss first the $pd \to pd$ process following Ref. [28]. In the $pd \to pd$ process there are three double-scattering amplitudes, which we denote symbolically as

$$M_{pp}(\mathbf{q}_1) \times M_{pn}(\mathbf{q}_2) + M_{pn}(\mathbf{q}_1) \times M_{pp}(\mathbf{q}_2) - M_{pn\to np}(\mathbf{q}_1) \times M_{np\to pn}(\mathbf{q}_2). \tag{7}$$

The small-angle charge-exchange scattering matrix $M_{pn\to np}$ can be rewritten in terms of the small-angle scattering matrices $M_{pp\to pp} \equiv M_{pp}$ and $M_{pn\to pn} \equiv M_{pn}$ in the form [31] $M_{pn\to np}(\mathbf{q}) = M_{np\to pn}(\mathbf{q}) = M_{pp}(\mathbf{q}) - M_{pn}(\mathbf{q})$. [The double-charge-exchange scattering matrix vanishes in the approximation $M_{pp}(\mathbf{q}) = M_{pn}(\mathbf{q})$, i.e. if one disregards the isospin dependence of the pN amplitude.] Therefore, the third term in Eq. (7) can be written as

$$\begin{aligned} &M_{pn\to np}(\mathbf{q}_1) \times M_{np\to pn}(\mathbf{q}_2) \\ &\quad = M_{pp}(\mathbf{q}_1) \times M_{pp}(\mathbf{q}_2) + M_{pn}(\mathbf{q}_1) \times M_{pn}(\mathbf{q}_2) \\ &\qquad - M_{pp}(\mathbf{q}_1) \times M_{pn}(\mathbf{q}_2) - M_{pn}(\mathbf{q}_1) \times M_{pp}(\mathbf{q}_2). \end{aligned} \tag{8}$$

The term $M_{pn\to np}(\mathbf{q}_1) \times M_{np\to pn}(\mathbf{q}_2)$ enters the full pd amplitude with opposite sign with respect to the first two terms given in Eq. (7) due to the additional permutation $p \leftrightarrow n$ in the deuteron vertex. Furthermore, the first and the second terms on the right-hand side of Eq. (8) constitute the term called the "charge-exchange" amplitude in Ref. [28] and are denoted by $A_i^{(c)}$. The third and the fourth terms from Eq. (8) can be absorbed into the first and second terms in Eq. (7), respectively, and this leads to the factor 2 in front of the $A_i^{(d)}$ amplitude in [28].

Coming back to the process $\bar{p}d \to \bar{p}d$, one should mention that in this case there are also three double-scattering terms in Eq. (2), namely

$$\begin{aligned} &M_{\bar{p}p}(\mathbf{q}_1) \times M_{\bar{p}n}(\mathbf{q}_2), \quad M_{\bar{p}n}(\mathbf{q}_1) \times M_{\bar{p}p}(\mathbf{q}_2), \\ &M_{\bar{p}p\to\bar{n}n}(\mathbf{q}_1) \times M_{\bar{n}n\to\bar{p}p}(\mathbf{q}_2). \end{aligned} \tag{9}$$

The first two terms constitute the amplitude $A_i^{(d)}$ in Eq. (6). The detailed formulas for $A_i^{(d)}$ ($i = 1, \ldots, 12$) coincide with those given in Table II of Ref. [28] for $pd \to pd$, where each term (A_N, B_N, C_N, C'_N, G_N, H_N) from the $pN \to pN$ amplitude ($N = p, n$) has to be replaced by the corresponding term of the scattering matrix $M_{\bar{p}N\to\bar{p}N}$ given in Eq. (3).

The last term in Eq. (9) gives rise to the $A_i^{(c)}$ amplitude in Eq. (6) and, like for the $pd \to pd$ process, enters the full amplitude also with the opposite sign with respect to the first two amplitudes in Eq. (9) for the same reason as in $pd \to pd$. In the present calculation the term with the charge-exchange amplitudes $\bar{p}p \leftrightarrow \bar{n}n$ is not expressed through the small-angle scattering amplitude, as in the $pd \to pd$ case, but calculated straightforwardly and, therefore, does not lead to the factor 2 in front of $A_i^{(d)}$ in Eq. (6) in contrast to Ref. [28]. The formulas for $A_i^{(c)}$ ($i = 1, \ldots, 12$) are the same as those given in Table III of Ref. [28], where each product $A_n(\mathbf{q}_2)A_n(\mathbf{q}_1)$, etc., has to be replaced by the corresponding terms $A_c(\mathbf{q}_2)A_c(\mathbf{q}_1)$, etc., of the charge-exchange scattering matrix $M_{\bar{p}p\leftrightarrow\bar{n}n}$. Finally, we want to emphasize that contrary to Ref. [28] the total double-scattering term enters Eq. (6) with positive sign. The relations of these amplitudes $A_i(q)$ with the spin observables considered in the present paper are given in the Appendix.

III. NUMERICAL RESULTS AND DISCUSSION

A. General remarks and differential observables

Earlier studies [26,27,32] and also our previous calculations [8,33] were all done within the spinless approximation for the elementary $\bar{p}N$ amplitude; i.e., they used only A_N from Eq. (3), parameterized in the Gaussian form, and they considered only the S-wave part of the wave function of the target nucleus. Those investigations suggested that the Glauber theory allowed one to explain the differential cross sections in the forward hemisphere and the total unpolarized cross section for the reactions $\bar{p}d$, $\bar{p}^3$He, and $\bar{p}^4$He even at rather low energies, i.e., down to 20–50 MeV of the incident antiproton. For $\bar{p}^4$He elastic scattering the first and the second diffraction peaks were explained by these calculations [33]. On the other hand, attempts to describe the second peak observed in $\bar{p}d$ elastic scattering at 179 MeV [34] were not quite that successful as documented in some papers [27,32].

In the present calculation we include the S- and D-wave components of the deuteron wave function and we keep the full spin dependence of the $\bar{p}N$ amplitude as given in Eq. (3). With regard to the wave function we use here the one of the CD-Bonn potential as parameterized in Ref. [35] and, for test calculations, also the one of the Paris potential [36]. The $\bar{p}N$ amplitude is taken from two models developed by the Jülich group, namely A(BOX) introduced in Ref. [9] and D described in Ref. [11]. Results for the total and integrated elastic ($\bar{p}p$) and charge-exchange ($\bar{p}p \to \bar{n}n$) cross sections and also for angular dependent observables for both models can be found in Refs. [9,11] while specific spin-dependent observables are presented in [12]. Model A as well as D provide a very good overall reproduction of the low- and intermediate-energy $\bar{N}N$ data as documented in those works.

An exemplary $\bar{p}d$ result demonstrating the role of the single-scattering (SS) and double-scattering (DS) mechanisms is presented in Fig. 2. There, cross sections based on the SS- and the DS mechanisms and their coherent sum (SS + DS) are displayed separately. One can see that the SS mechanism alone fails to explain the forward peak. However, the sum SS + DS describes it rather well. Obviously, the DS mechanism, neglected in Ref. [8] in the calculation of the spin-dependent total cross sections, has a sizable influence even in the region of the forward peak.

When accounting for the spin dependence of the $\bar{p}N$ interaction one has to address also the reliability of the employed Glauber approach, specifically, as far as the angular range is concerned. In contrast to the spin-independent part of the amplitude Eq. (3) given by A_N ($N = p, n$), most of the other amplitudes that give rise to the spin dependence [B_N, C_N, C'_N, G_N, H_N in Eq. (3)] do not exhibit a very pronounced diffractive behavior for antiproton beam energies 50–200 MeV; i.e., they do not decrease rapidly with increasing center-of-mass (c.m.) scattering angle $\theta_{c.m.}$. In fact, some of these amplitudes even increase with increasing $\theta_{c.m.}$ and their magnitude is larger at $\theta_{c.m.} > 90^\circ$ than at $\theta_{c.m.} < 90^\circ$. The typical behavior of the differential $\bar{p}N$ cross section can be seen in Fig. 3 for 179 MeV. This behavior is basically the same for both Jülich models A and D and, therefore, we consider only model D in the following. The visible rise of

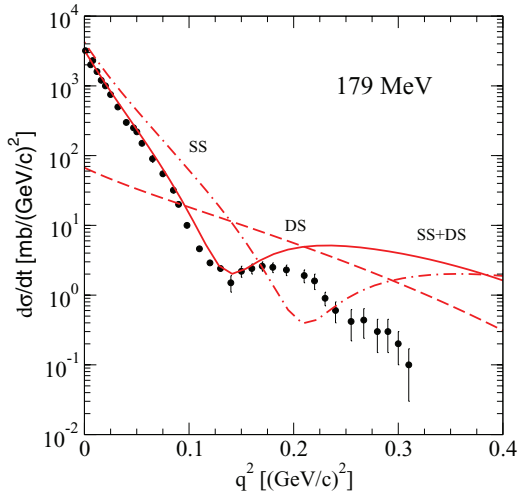

FIG. 2. (Color online) Differential cross section of elastic $\bar{p}d$ scattering at 179 MeV versus the transferred momentum squared. Results based on single-scattering (dash-dotted line), double-scattering (dashed), and the full (solid) Glauber mechanisms are shown. For the calculation the $\bar{p}N$ amplitude predicted by the Jülich model D is utilized. The data points are from Ref. [34].

the cross section for backward angles is partly due to those spin-dependent pieces of the $\bar{p}N$ amplitude and is reflected in the corresponding $\bar{p}d$ results by the appearance of a second, broad peak at large transferred momenta $q^2 \sim 0.35$ (GeV/c)^2 coming from the SS contribution alone, as is seen in Fig. 2. As a consequence, the second ("diffraction") peak that appears in the full calculation, including now the SS and DS mechanisms, originates not only from the interference between the SS and DS amplitudes, as is usually the case for typical diffractive scattering, but is also related to that backward peak seen in the cross section of the (elementary) $\bar{p}N$ reaction. We confirmed in test calculations within the SS mechanism, utilizing just the amplitudes A_N in Eq. (3) or a standard Gaussian-type representation of the total $\bar{p}N$ amplitude in the spinless

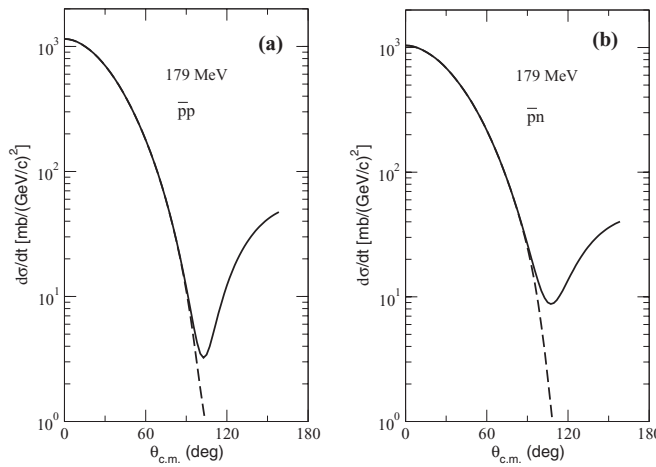

FIG. 3. Differential elastic $\bar{p}p$ (a) and $\bar{p}n$ (b) cross sections at 179 MeV as predicted by model D (solid lines). The dashed line shows the result with the smooth cutoff with $q_0^2 = 0.21$ GeV/c and $\nu = 10$, corresponding to $\theta_{c.m.}^{\bar{p}N} = 105^\circ$, as explained in the text.

approximation, that then the differential cross sections do not demonstrate this behavior.

One should note that the Glauber diffraction theory of multistep scattering is not suitable for taking into account backward scattering in the elementary hadron-nucleon collision, because its basis is the eikonal approximation. The deuteron elastic form factor suppresses the contribution of the $\bar{p}N$ amplitudes at large angles, but at the considered low and moderate energies this effect is not as strong as at significantly higher energies for the same scattering angle.

The authors of Refs. [28,29] approximate all amplitudes in Eq. (3) as a sum of Gaussians, e.g.,

$$A_N(q) = \sum_{j=1}^{n} c_{A_N,j} \exp(-d_{A_N,j}\, q^2), \quad \text{etc.}, \tag{10}$$

where $c_{A_N,j}$ and $d_{A_N,j}$ are parameters fixed by a fit to the original NN amplitudes. With such a series of Gaussians they are able to reproduce the original amplitudes quite well in the forward hemisphere, i.e., up to angles of $\theta_{c.m.} = 80^\circ$–90°, as reported in [29]. For larger angles the differential NN cross section based on those Gaussians drop off very quickly, in accordance with the requirements by the Glauber model, as shown in Fig. 4 of Ref. [29]. However, it remains unclear how and, specifically, how fast the individual (parameterized) amplitudes drop off. In particular, issues such as the influence of the backward tail on the results, or the related question of up to which angles one can trust the predictions for pd observables, are not addressed in Ref. [28].

In the following we investigate this subject in the context of elastic $\bar{p}d$ scattering. For this purpose we perform various calculations of this reaction within the Glauber theory in order to scrutinize the sensitivity of the considered $\bar{p}d$ observables to the large-angle region of the employed elementary $\bar{p}N$ amplitudes. Clearly, any such sensitivity is in contradiction with the assumptions of the Glauber theory and tells us that the corresponding $\bar{p}d$ results are no longer reliable. We use also a Gaussian ansatz for representing the amplitudes generated by the $\bar{N}N$ models A and D in analytical form. However, we aim at an excellent reproduction of the original amplitudes over the whole angular range. This means that typically we have to use 10 or even 12 terms in the sum in Eq. (10), instead of $n = 5$ which was taken in [28,29].

We examine the sensitivity by varying the large-angle behavior of the $\bar{N}N$ amplitudes that enter our Glauber calculation for $\bar{p}d$. In a first series of calculations a *smooth cutoff* on the angular region is introduced by multiplying the employed $\bar{p}N$ amplitude by the factor $F(q) = 1/[1 + (q^2/q_0^2)^\nu]$. This is done in the evaluation of the SS mechanism as well as for the DS mechanism, i.e. in the two-dimensional integral in Eq. (6). The lowest value for the cutoff momentum q_0 is chosen in such a way that it corresponds to a $\bar{p}N$ c.m. scattering angle which is close to the position of the minimum of the elementary $\bar{p}N$ cross section. For the case of 179 MeV, shown in Fig. 3 (see dashed line), this amounts to $\theta_{c.m.} \approx 105^\circ$. This choice for q_0 makes sure that at least the $\bar{p}N$ cross section produced by those modified $\bar{p}N$ amplitudes shows a clear diffractive behavior. We then increase the cutoff momentum q_0 until the corresponding angle $\theta_{c.m.}$ reached 180 degrees. In the actual calculations the exponent ν was varied in the range $\nu = 10$–15.

As an alternative to variations of q_0 we performed also calculations with a *sharp cutoff* at the maximum transferred momentum in the physical region $q = 2k_{\bar{p}N}$, where $k_{\bar{p}N}$ is the $\bar{p}N$ c.m. momentum.

Finally, we employed different Gaussian parametrizations, varying the number of terms between 6 and 12, and without cutoff. Those parametrizations of the $\bar{p}N$ amplitudes differ from the ones considered above in the angular range $90^\circ \leqslant \theta_{c.m.} \leqslant 180^\circ$ but, more importantly, for larger transferred momenta q outside of the physical range, i.e., $q > 2k_{\bar{p}N}$. Note that the integration in Eq. (6) requires the $\bar{p}N$ amplitudes at any (large) q; however, as already said above, the deuteron wave function strongly suppresses contributions to the integral from that region.

The result of our analysis is summarized in Figs. 4–9. The bands represent the variation of the calculated $\bar{p}d$ observables due to the cutoff procedures described above. We regard these bands as a sensible guideline for estimating the angular region where the Glauber theory is able to provide solid results for a specific observable and where this approach starts to fail. In particular, they indicate when contributions from large angles start to become significant. Since such contributions are in contradiction with the basic approximations underlying the Glauber model, any sizable influence from them undoubtedly marks the breakdown of this approach.

The above considerations suggest that within the Glauber approach reliable predictions can be obtained for the differential cross section (Figs. 4–6) and also for the spin observables A_y^d, $A_y^{\bar{p}}$, A_{xx}, and A_{yy} (Figs. 7, 8, and 9) for c.m. scattering angles up to 50°–60° in the $\bar{p}d$ system. Obviously, within this angular region there is practically no sensitivity to the $\bar{p}N$ amplitudes in the backward hemisphere, in accordance with the requirements of the Glauber approach. As expected, for

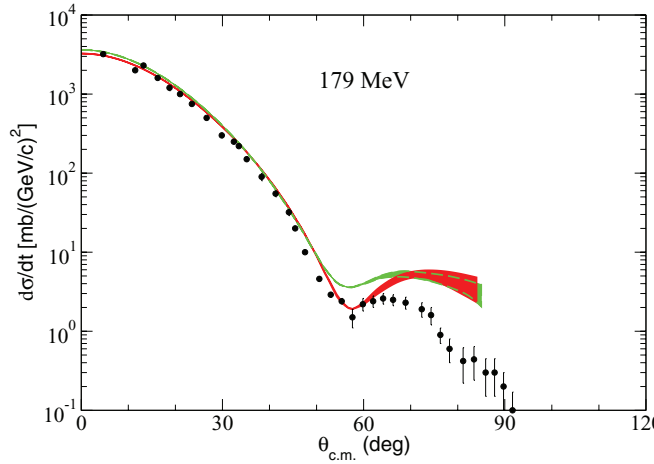

FIG. 4. (Color online) Differential cross section of elastic $\bar{p}d$ scattering at 179 MeV versus the c.m. scattering angle. Results of our full calculation (including the SS + DS mechanisms) are shown based on the $\bar{N}N$ models model A (green/grey) and D (red/black). The bands represent the sensitivy to variations of the large-angle tail of the $\bar{p}N$ amplitudes as discussed in the text. The data points are taken from Ref. [34].

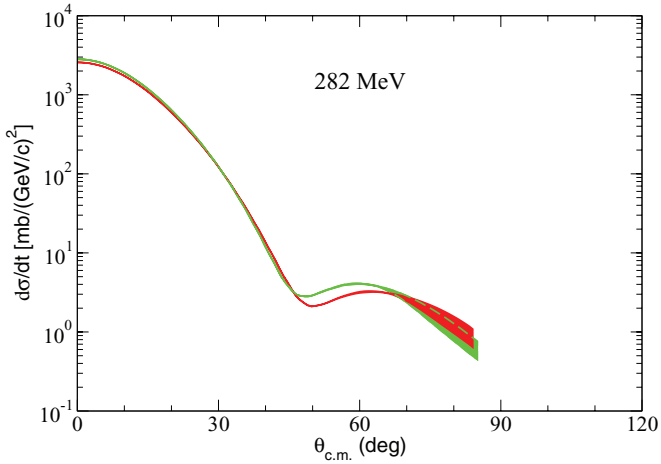

FIG. 5. (Color online) Differential cross section of elastic $\bar{p}d$ scattering at 282 MeV versus the c.m. scattering angle. Same description of curves as in Fig. 4.

larger angles where such a sensitivity is observed, the width of the corresponding bands are smaller for higher energies (Fig. 5) and larger at lower energies (Fig. 6). This feature can be seen in case of the differential cross sections and also for the spin observables A_y, A_{yy}, A_{xx} presented in Figs. 7, 8, and 9.

A comparison of our calculation with experimental data is only meaningful for such $\bar{p}d$ scattering angles where the Glauber approach works well. According to our calculations this region includes the whole diffractive peak in the differential cross section $d\sigma/dt$ at forward angles, for energies from around 50 MeV upwards. This finding is important for the issue of the polarization buildup of antiprotons, because it validates the application of the optical theorem for evaluating the total polarized cross sections based on the obtained forward $\bar{p}d$ amplitude.

With regard to the measured differential cross section at 179 MeV, see Fig. 4, our Glauber calculation describes quite well the first diffractive peak, for $\bar{p}N$ amplitudes generated from model A as well as for those of model D.

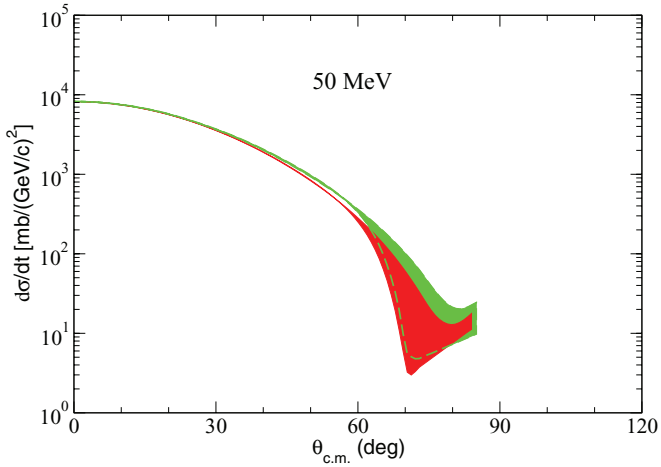

FIG. 6. (Color online) Differential cross section of elastic $\bar{p}d$ scattering at 50 MeV versus the c.m. scattering angle. Same description of curves as in Fig. 4.

The first minimum in the differential cross section, located at $q^2 \approx 0.12$–0.13 $(\mathrm{GeV}/c)^2$ (i.e. $\theta_{c.m.} \approx 55^\circ$), and the onset of the second maximum, are explained only by model D. The obvious strong disagreement with the data at larger transferred momenta, $q^2 > 0.15$ $(\mathrm{GeV}/c)^2$, corresponding to $\theta_{c.m.} > 60^\circ$, lies already in the region where the Glauber theory cannot be applicable anymore—for the case of the spinless approximation for the $\bar{p}N$ amplitudes as well as when the spin-dependent amplitudes are included—and, therefore, no conclusions can be drawn. Note that at lower energies, specifically at 50 MeV, the first minimum lies outside of the region where the Glauber approach can be trusted. In this context let us also mention that the results shown in Fig. 2 were obtained without any cutoff.

Some remarks on the spin-dependent observables presented in Figs. 7, 8, and 9: The results obtained for the vector analyzing powers $A_y^{\bar{p}}$ and A_y^d indicate a strong model dependence. In contrast, the tensor analyzing powers A_{xx} and A_{yy} exhibit a very similar behavior for both models A and D. We found that the spin-independent amplitudes dominate the latter observables and the inclusion of the spin-dependent amplitudes has only a minor influence. Thus, the results obtained here for A_{xx} and A_{yy} seem to be quite robust up to scattering angles of 60°–70°. When the spin-dependent terms of the elementary $\bar{p}N$ amplitude (B_N, C_N, C'_N, G_N, H_N) are excluded, then the vector analyzing powers $A_y^{\bar{p}}$ and A_y^d vanish.

At 50 MeV the uncertainties in the considered spin-dependent observables increase dramatically for angles around 65°, in accordance with the strong variations that one sees in the differential cross section (Fig. 6), and, therefore, we do not show those quantities beyond 70°.

We looked also at the influence of the D-wave component of the deuteron on the obtained results. In the differential cross section the contribution due to the D wave is rather small in the forward direction, but increases with increasing scattering angle. For example, at 179 MeV the contribution by the D wave amounts to around 30% of the absolute value in the region of the first minimum. The tensor analyzing powers A_{xx} and A_{yy} are considerably reduced (by one order of magnitude) when the D wave is neglected. Actually, these observables practically vanish if, in addition, the spin-dependent terms of the elementary $\bar{p}N$ amplitude are omitted. For observables that exhibit a larger sensitivy to the D-wave component, we performed also test calculations with the wave function of the Paris potential which has a somewhat larger D-wave probability [36]. It turned out that the sensitivity to differences in wave functions is, in general, fairly small. Even in case of those tensor analyzing powers they amount to variations in the order of 2%–4% only and they occur predominantly at the minima (maxima).

B. Total spin-dependent cross sections

The total $\bar{p}d$ cross section is defined by [8]

$$\sigma_{\mathrm{tot}} = \sigma_0 + \sigma_1 \mathbf{P}^{\bar{p}} \cdot \mathbf{P}^d + \sigma_2 (\mathbf{P}^{\bar{p}} \cdot \hat{\mathbf{k}})(\mathbf{P}^d \cdot \hat{\mathbf{k}}) + \sigma_3 P_{zz}, \qquad (11)$$

where $\hat{\mathbf{k}}$ is the unit vector in the direction of the antiproton beam, $\mathbf{P}^{\bar{p}}$ ($\mathbf{P}^d$) is the polarization vector of the antiproton (deuteron), and P_{zz} is the tensor polarization of the deuteron ($OZ||\hat{\mathbf{k}}$). The total unpolarized cross section σ_0 and the spin-

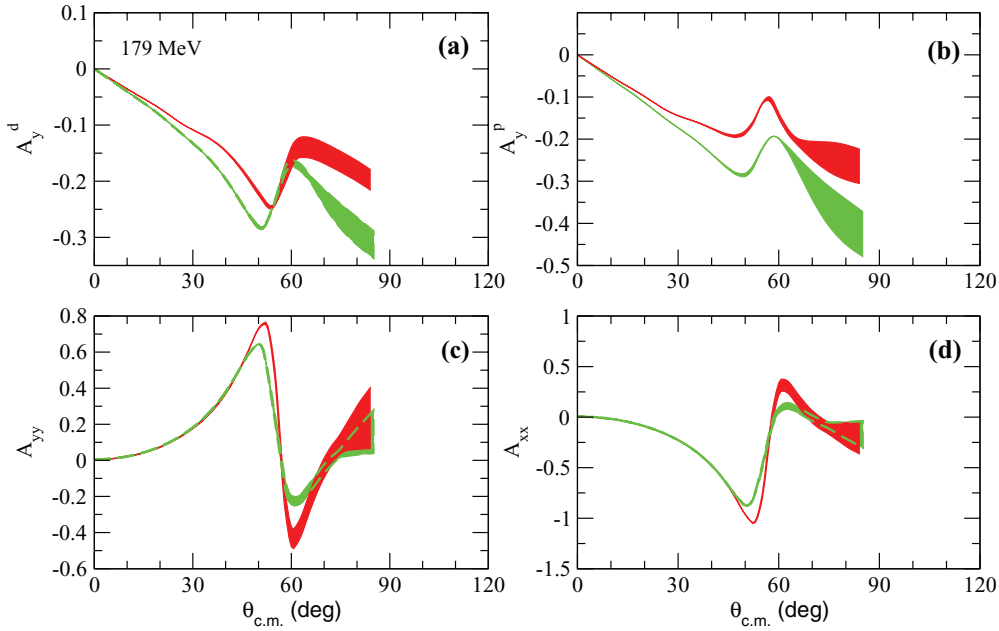

FIG. 7. (Color online) Spin observables of elastic $\bar{p}d$ scattering at 179 MeV versus the c.m. scattering angle: A_y^d (a), $A_y^{\bar{p}}$ (b), A_{yy} (c), and A_{xx} (d). Results of our full calculation (including the SS + DS mechanisms) are shown based on the $\bar{N}N$ models model A (green/grey) and D (red/black). The bands represent the sensitivity to variations of the large-angle tail of the $\bar{p}N$ amplitudes as discussed in the text.

dependent cross sections σ_i ($i = 1, 2, 3$) are calculated using the generalized optical theorem as described in Ref. [8]. Note, however, that erroneous expressions for the σ_i have been given and used in that work [in Eqs. (19)-(20)]. Specifically, the correct σ_1 and σ_2 which are shown in the present work are of opposite sign to those given in Ref. [8], see the Appendix for details and for the correct expressions.

Results for the total unpolarized $\bar{p}d$ cross section are displayed in Fig. 10 together with experimental information [37–41]. Obviously the unpolarized cross section is described rather well by both Jülich models A and D [11] within the SS + DS mechanisms (dashed and solid lines, respectively), while it is overestimated by $\sim$10%–15% within the SS approximation, exemplified in Fig. 10 only for model D (dash-dotted line). A similar result was obtained in the spinless approximation in Ref. [8]. Taking into account the double-scatterig mechanism leads to more sizable changes in the results for the spin-dependent cross section, relevant for

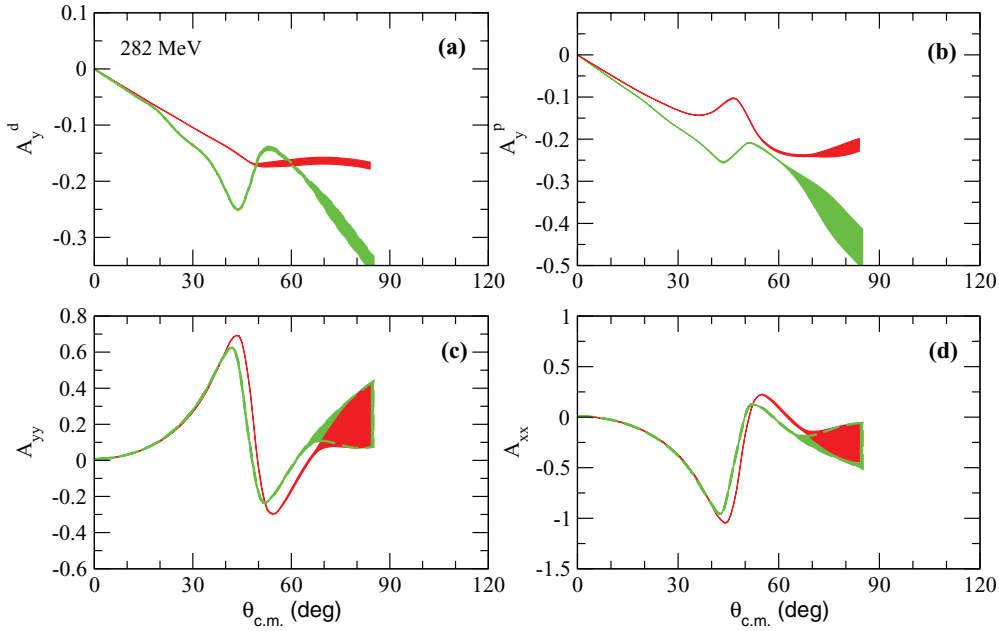

FIG. 8. (Color online) Spin observables of elastic $\bar{p}d$ scattering at 282 MeV versus the c.m. scattering angle. Same description of curves as in Fig. 7.

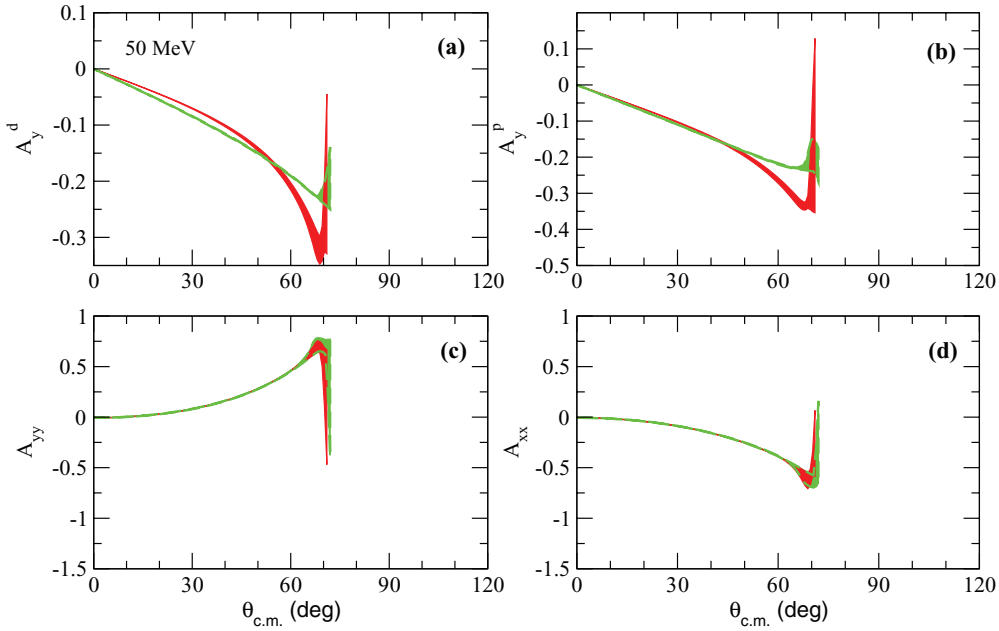

FIG. 9. (Color online) Spin observables of elastic $\bar{p}d$ scattering at 50 MeV versus the c.m. scattering angle. Same description of curves as in Fig. 7.

the spin-filtering mechanism (see Figs. 11 and 12), especially for σ_2. One can see from Fig. 12 that this cross section is reduced by roughly a factor of two when the double-scattering mechanism is included. For the cross section σ_1 this difference is in the order of 10%–15%. Note that a decrease of the absolute values of σ_0, σ_1, and σ_2, due to shadowing effects, of comparable magnitude was reported in Ref. [13] in a calculation based on the Nijmegen $\bar{p}N$ amplitudes [14].

The cross sections σ_0, σ_1, and σ_2 are more or less completely determined by the $\bar{p}N$ at forward angles and, thus, can be reliably calculated within the Glauber approach. Indeed, the uncertainty bands turned out to be very small and, therefore, we do not show them in the figures. The tensor polarized cross section σ_3, shown in Fig. 13, vanishes in the SS approximation. At low energies 25–50 MeV this cross section is in the order of 2 mb. Unlike the other cross sections discussed above, σ_3 turned out to be fairly sensitive to the values of the $\bar{p}N$ amplitudes at large angles, i.e., to the variations considered in Sec. III A. Thus, there is a significant uncertainty in the predictions based on the Glauber theory as indicated by the bands. With increasing energy the cross section σ_3 decreases and is only about 0.3–0.5 mb above 100 MeV. As expected, at

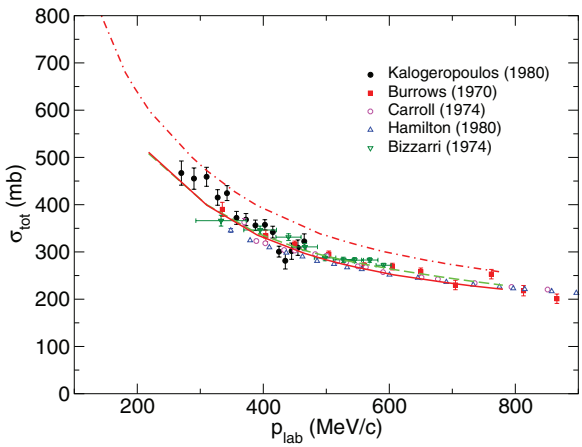

FIG. 10. (Color online) Total unpolarized $\bar{p}d$ cross section versus the antiproton laboratory momentum. Results of our full calculation (including the SS + DS mechanisms) are shown based on the $\bar{N}N$ models A (dashed line) and D (solid line). The result obtained for the SS mechanism alone based on model D is indicated by the dash-dotted line. Data are taken from Refs. [37–41].

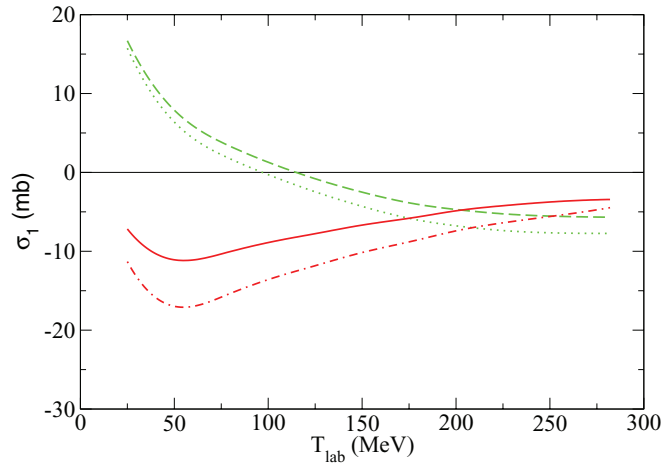

FIG. 11. (Color online) Total $\bar{p}d$ cross section σ_1 versus the antiproton kinetic energy in the laboratory system. Results are shown based on the $\bar{N}N$ models A (green/grey) and D (red/black). Calculations for the SS mechanism alone are indicated by dotted (A) and dash-dotted (D) lines while the full calculations (SS + DS mechanisms) are given by the dashed (A) and solid (D) lines.

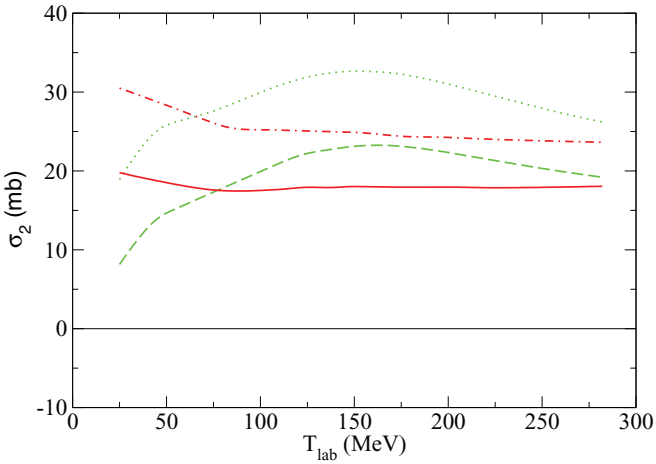

FIG. 12. (Color online) Total $\bar{p}d$ cross section σ_2 versus the antiproton kinetic energy in the laboratory system. Same description of curves as in Fig. 11.

higher energies the sensitivity to the $\bar{p}N$ amplitudes at large angles decreases too.

With regard to the influence of the D-wave component of the deuteron wave function on the total cross sections, we found that its contribution to σ_1 and σ_2 is less than 1% for both considered $\bar{N}N$ models. The total unpolarized cross section σ_0 decreases by $\sim$5% if the D wave is neglected. The cross section σ_3, which is nonzero only if the double-scattering mechanism is accounted for, is very sensitive to the D-wave component. If the D wave is neglected, then σ_3 changes significantly and, specifically, remains positive over the whole considered energy range. On the other hand, we observe only minor variations when using the Paris deuteron wave function instead of the one of the CD-Bonn potential. They are smaller

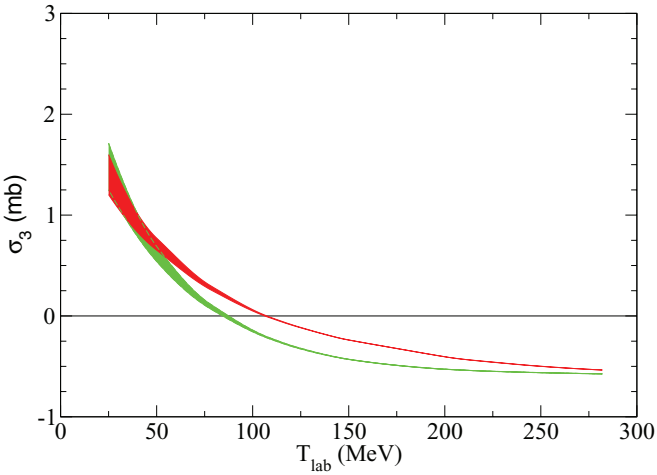

FIG. 13. (Color online) Total $\bar{p}d$ cross section σ_3 versus the antiproton kinetic energy in the laboratory system. Results of our full calculation (including the SS + DS mechanisms) are shown based on the $\bar{N}N$ models model A (green/grey) and D (red/black). The bands represent the sensitivy to variations of the large-angle tail of the $\bar{p}N$ amplitudes as discussed in the text.

than the uncertainties of our predictions indicated by the bands in Fig. 13.

C. Polarization efficiency

According to the analysis of the kinetics of polarization [5,42], the polarization buildup is determined mainly by the ratio of the polarized total cross sections to the unpolarized one [5]. Let us define the unit vector $\boldsymbol{\zeta} = \mathbf{P}_T/P_T$, where $\mathbf{P}_T = \mathbf{P}^d$ is the target polarization vector which enters Eq. (11). The nonzero antiproton beam polarization vector $\mathbf{P}^{\bar{p}}$, produced by the polarization buildup, is collinear to the vector $\boldsymbol{\zeta}$ for any directions of $\mathbf{P}_T$ and can be calculated from consideration of the kinetics of polarization. The general solution for the kinetic equation for $\bar{p}p$ scattering is given in Ref. [5]. Here we assume that this solution is valid for $\bar{p}d$ scattering also. Therefore, for the spin-filtering mechanism of the polarization buildup the polarization degree at the time t is given by [5,43]

$$P_{\bar{p}}(t) = \tanh\left[\frac{t}{2}(\Omega_-^{\text{out}} - \Omega_+^{\text{out}})\right], \tag{12}$$

where

$$\Omega_\pm^{\text{out}} = nf\{\sigma_0 \pm P_T[\sigma_1 + (\boldsymbol{\zeta}\cdot\hat{\mathbf{k}})^2\sigma_2]\}. \tag{13}$$

Here n is the areal density of the target and f is the beam revolving frequency. Note that the cross sections in Eq. (13) involve hadronic as well as Coulomb contributions; see, e.g., Refs. [5,8]. Obviously the tensor cross section σ_3 from Eq. (11) does not contribute to $\Omega_\pm^{\text{out}}$. Assuming the condition $|\Omega_-^{\text{out}} - \Omega_+^{\text{out}}| \ll (\Omega_-^{\text{out}} + \Omega_+^{\text{out}})$, which was found in Refs. [5,43] for $\bar{p}p$ scattering in rings at $n = 10^{14}$ cm^{-2} and $f = 10^6 c^{-1}$, one can simplify Eq. (12). If one denotes the number of antiprotons in the beam at the time moment t as $N(t)$, then the figure of merit is $P_{\bar{p}}^2(t)N(t)$. This value is maximal at the moment $t_0 = 2\tau$, where τ is the beam lifetime. The latter is determined by σ_0, the total cross section of the interaction of the antiprotons with the deuteron target, via

$$\tau = \frac{1}{nf\sigma_0}. \tag{14}$$

The quantity relevant for the efficiency of the polarization buildup is the polarization degree $P_{\bar{p}}$ at the time t_0 [43]. In our definition for σ_1 and σ_2, which differs from that in Refs. [5,43], we find

$$\begin{aligned} P_{\bar{p}}(t_0) &= -2P_T\frac{\sigma_1}{\sigma_0}, \quad \text{if} \quad \boldsymbol{\zeta}\cdot\hat{\mathbf{k}} = 0\,, \\ P_{\bar{p}}(t_0) &= -2P_T\frac{\sigma_1+\sigma_2}{\sigma_0}, \quad \text{if} \quad |\boldsymbol{\zeta}\cdot\hat{\mathbf{k}}| = 1. \end{aligned} \tag{15}$$

For evaluating the polarization degree, Coulomb effects are taken into account via the procedure described in Ref. [8]. Thus the quantities σ_i ($i = 0, 1, 2$) in Eq. (15) are actually the sum of the hadronic cross sections, of the Coulomb cross section (only for $i = 0$), and of the Coulomb nuclear interference terms. In the concrete calculation an acceptance angle of 20 mrad is used.

The polarization degree $P_{\bar{p}}(t_0)$ for $\boldsymbol{\zeta}\cdot\hat{\mathbf{k}} = 1$ ($P_{||}$) at $P_T = P^d = 1$ is shown in Fig. 14 together with the results for

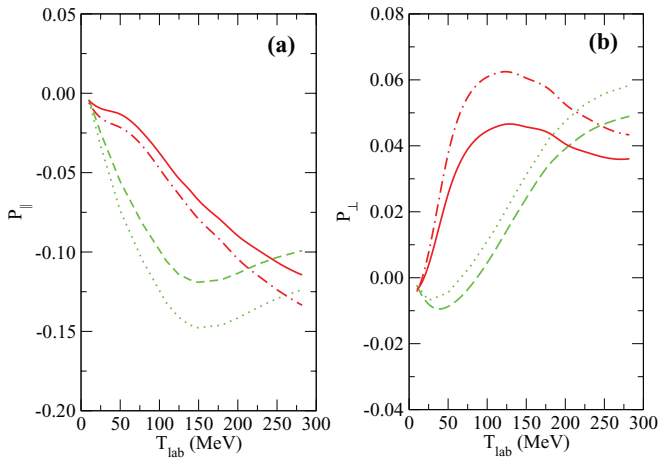

FIG. 14. (Color online) Dependence of the longitudinal [$P_{||}$, panel (a)] and transverse [$P_\perp$, panel (b)] polarization on the beam energy. Same description of curves as in Fig. 11. The acceptance angle is 20 mrad.

$\boldsymbol{\zeta} \cdot \hat{\mathbf{k}} = 0$ ($P_\perp$). One can see that, in general, the polarization efficiency increases with increasing energy. For longitudinal polarization maximal values of about 10%–15% are predicted above 150 MeV; see Fig. 14(a). The transverse polarization degree is smaller than the longitudinal one for both models A and D. Of course, as was already pointed out in our earlier works [8,44], there is a significant model dependence in the predictions for both polarization cases.

Obviously, the inclusion of the DS mechanism leads to a decrease of the longitudinal $P_{||}$ as well as of the transverse $P_\perp$ polarization efficiencies by about 20%–30% as compared to the SS mechanism alone [33]. Nevertheless, for both considered models the magnitude of the spin-dependent cross sections is still comparable or even larger than those for $\bar{p}p$ [8,43,44]. In this context let us also mention that the values for the polarization degree we obtained are somewhat smaller than those presented in [13], based on the Nijmegen $\bar{N}N$ partial wave analysis [14] from 1994.

Finally, in Fig. 15 we document the dependence of the quantities $P_{||}$ and $P_\perp$ on the acceptance angle. As expected, in general the polarization degree increases with increasing acceptance angle. But the variations themselves are not too dramatic.

IV. SUMMARY

In the present work we analyzed the role of the spin dependence of the $\bar{p}N$ amplitude in elastic $\bar{p}d$ scattering for energies of 50–300 MeV of the incident antiproton on the basis of the Glauber theory. In the actual calculations we utilized elementary $\bar{p}N$ amplitudes generated from the Jülich $\bar{N}N$ model [11]. The S- and D-wave components of the deuteron were included in the calculation and the single- and double-scattering mechanisms were taken into account.

Since some of the spin-dependent amplitudes exhibit a nondiffractive behavior we performed various test calculations in order to pin down the angular range where the Glauber theory can be reliably applied. Thereby, it turned out that this approach works rather well for the region of the forward peak, over the whole considered energy region. Obviously, for the considered $\bar{p}N$ models those amplitudes with nondiffractive character are fairly small as compared to the dominant spin-independent amplitude (with a pronounced diffractive behavior) so that the former do not spoil the applicability of the Glauber theory. This means, in turn, that the approach can be used safely for the calculation of the total spin-dependent $\bar{p}d$ cross sections

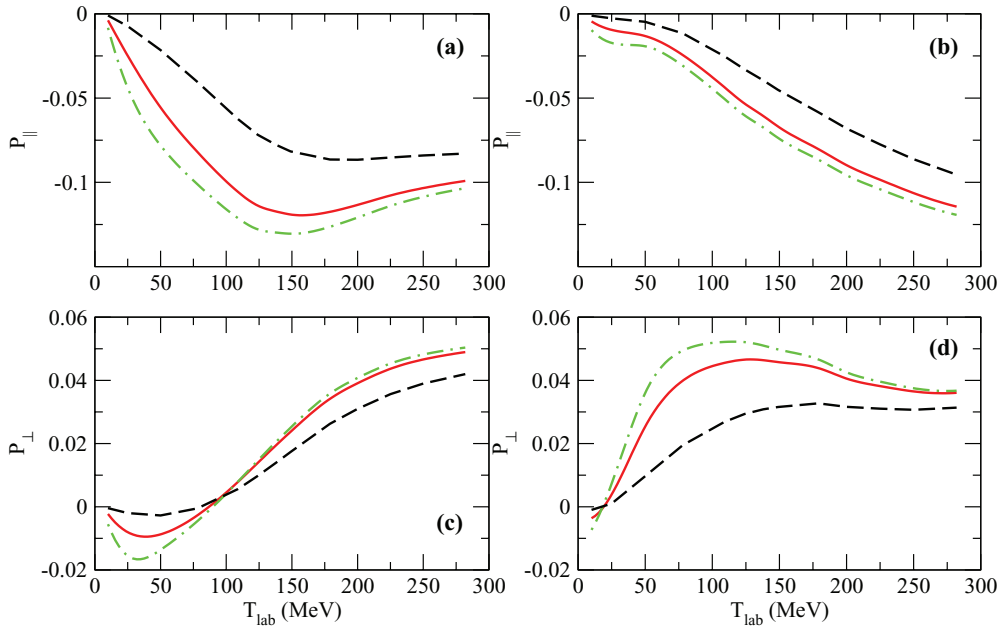

FIG. 15. (Color online) Dependence of the longitudinal [$P_{||}$, panels (a) and (b)] and transverse [$P_\perp$, panels (c) and (d)] polarization on the acceptance angle, for the $\bar{N}N$ model A [(a) and (c)] and model D [(b) and (d)]. The dashed, solid, and dash-dotted curves are results for acceptance angles of 10, 20, and 30 mrad, respectively.

via the optical theorem. With regard to the considered $\bar{p}d$ differential cross sections and vector and tensor analyzing powers (A_y^d, $A_y^{\bar{p}}$, A_{yy}, A_{xx}), our investigation indicates that reliable predictions can be obtained for c.m. scattering angles up to 50°–60° in the $\bar{p}d$ system. For 179 MeV, where data on the differential cross section exist, this range covers the first minimum and the onset of the second maximum. Here our results based on the $\bar{p}N$ amplitudes of the Jülich model D turned out to agree nicely with the experiment, while model A overestimates the measured $\bar{p}d$ cross section at the minimum.

The total polarized $\bar{p}d$ cross sections σ_i ($i = 1, 2, 3$), and specifically the polarization degree of the antiproton beam, are of interest in the context of plans to establish a polarized antiproton beam via the spin-filtering method as proposed by the PAX Collaboration (see also [45]). Corresponding predictions presented in this work exhibit a sizable model dependence, reflecting the uncertainties in the spin dependence of the elementary $\bar{p}p$ and $\bar{p}n$ interactions. Still, for both considered models we find that the magnitude of the spin-dependent cross sections is comparable or even larger than those for $\bar{p}p$. Thus, our results suggest that deuteron targets can be used for the polarization buildup of antiprotons at beam energies of 100–300 MeV with similar and possibly even higher efficiency than $\bar{p}p$ scattering. Nonetheless, only concrete experimental data on the spin-dependent part of the cross sections of $\bar{p}p$ and $\bar{p}d$ scattering will allow one to confirm or disprove the feasibility of the spin filtering mechanism for the antiproton polarization buildup.

ACKNOWLEDGMENTS

We acknowledge stimulating discussions with N. N. Nikolaev and F. Rathmann. We would like to thank V. I. Kukulin and M. N. Platonova for communicating more details concerning the work published in [28,29]. This work was supported in part by the WTZ Project No. 01DJ12057.

APPENDIX: INVARIANT AMPLITUDES A_i AND SPIN OBSERVABLES FOR $\bar{p}d$ ELASTIC SCATTERING

The scattering matrix $M_{\bar{p}d}$ in Eq. (1) can be expressed via the 12 invariant amplitudes A_i in the following way [28]:

$$\begin{aligned} M_{\bar{p}d} = {} & (A_1 + A_2\boldsymbol{\sigma}\cdot\hat{\mathbf{n}}) + (A_3 + A_4\boldsymbol{\sigma}\cdot\hat{\mathbf{n}})(\mathbf{S}\cdot\hat{\mathbf{q}})^2 \\ & + (A_5 + A_6\boldsymbol{\sigma}\cdot\hat{\mathbf{n}})(\mathbf{S}\cdot\hat{\mathbf{n}})^2 + (A_7\boldsymbol{\sigma}\cdot\hat{\mathbf{k}})(\mathbf{S}\cdot\hat{\mathbf{k}}) \\ & + (A_8\boldsymbol{\sigma}\cdot\hat{\mathbf{q}})[(\mathbf{S}\cdot\hat{\mathbf{q}})(\mathbf{S}\cdot\hat{\mathbf{n}}) + (\mathbf{S}\cdot\hat{\mathbf{n}})(\mathbf{S}\cdot\hat{\mathbf{q}})] \\ & + (A_9 + A_{10}\boldsymbol{\sigma}\cdot\hat{\mathbf{n}})(\mathbf{S}\cdot\hat{\mathbf{n}}) + (A_{11}\boldsymbol{\sigma}\cdot\hat{\mathbf{q}})(\mathbf{S}\cdot\hat{\mathbf{q}}) \\ & + (A_{12}\boldsymbol{\sigma}\cdot\hat{\mathbf{k}})[(\mathbf{S}\cdot\hat{\mathbf{k}})(\mathbf{S}\cdot\hat{\mathbf{n}}) + (\mathbf{S}\cdot\hat{\mathbf{n}})(\mathbf{S}\cdot\hat{\mathbf{k}})]\,. \end{aligned} \tag{A1}$$

Here $\mathbf{S} = (\boldsymbol{\sigma}_p + \boldsymbol{\sigma}_n)/2$ is the total spin of the deuteron and the definition of the unit vectors $\hat{\mathbf{k}}$, $\hat{\mathbf{q}}$, and $\hat{\mathbf{n}}$ is given right after Eq. (3). In the coordinate system as chosen in Ref. [28], with the axes $\hat{\mathbf{e}}_\mathbf{x} = \hat{\mathbf{q}}$, $\hat{\mathbf{e}}_\mathbf{y} = \hat{\mathbf{n}}$, and $\hat{\mathbf{e}}_\mathbf{z} = \hat{\mathbf{k}}$, the differential cross section $d\sigma/dt$ and analyzing powers $A_y^{\bar{p}}$, A_y^d, A_{xx}, and A_{yy} take the following forms [28]:

$$\begin{aligned} d\sigma/dt \equiv \tfrac{1}{3}\Sigma = {} & |A_1|^2 + |A_2|^2 + \tfrac{2}{3}\{Z + Re[2A_1^*(A_3 + A_5) \\ & + 2A_2^*(A_4 + A_6) + A_3^*A_5 + A_4^*A_6]\}, \end{aligned} \tag{A2}$$

where $Z = \sum_{i=3}^{12} |A_i|^2$,

$$\begin{aligned} A_y^{\bar{p}} = {} & 2\,\mathrm{Re}[2(A_1^* + A_3^* + A_5^*)(A_2 + A_4 + A_6) \\ & + A_1^*A_2 - A_3^*A_6 - A_4^*A_5 + 2A_9^*A_{10}]\Sigma^{-1}, \end{aligned} \tag{A3}$$

$$\begin{aligned} A_y^d = {} & 2\,\mathrm{Re}[(2A_1^* + A_3^* + 2A_5^*)A_9 + (2A_2^* + A_4^* \\ & + 2A_6^*)A_{10} + A_7^*A_{12} + A_8^*A_{11}]\Sigma^{-1}, \end{aligned} \tag{A4}$$

$$\begin{aligned} A_{yy} = {} & \{2(|A_5|^2 + |A_6|^2 + |A_9|^2 + |A_{10}|^2) \\ & - (|A_3|^2 + |A_4|^2 + |A_7|^2 + |A_8|^2 + |A_{11}|^2 + |A_{12}|^2) \\ & + 2\,\mathrm{Re}[A_1^*(2A_5 - A_3) + A_2^*(2A_6 - A_4) \\ & + A_3^*A_5 + A_4^*A_6]\}\Sigma^{-1}, \end{aligned} \tag{A5}$$

$$\begin{aligned} A_{xx} = {} & \{2(|A_3|^2 + |A_4|^2 + |A_{11}|^2 + |A_{12}|^2) \\ & - (|A_5|^2 + |A_6|^2 + |A_7|^2 + |A_8|^2 + |A_9|^2 + |A_{10}|^2) \\ & + 2\,\mathrm{Re}[A_1^*(2A_3 - A_5) + A_2^*(2A_4 - A_6) \\ & + A_3^*A_5 + A_4^*A_6]\}\Sigma^{-1}. \end{aligned} \tag{A6}$$

The amplitudes A_i can be rewritten as linear combinations of the amplitudes F_i used in our previous paper [8]. The latter are defined within a different basis as compared to Eq. (A1). In terms of the amplitudes F_i the observables given in Eqs. (A2)–(A6) coincide with those given in the Appendix of Ref. [8]. For collinear kinematics ($q = 0$) the scattering matrix $M_{\bar{p}d}(0)$ contains four independent terms [46] and can be written as [47]

$$\begin{aligned} M_{\bar{p}d;\alpha\beta}(0) = {} & g_1\delta_{\alpha\beta} + (g_2 - g_1)\hat{k}_\alpha\hat{k}_\beta + ig_3\sigma_i\epsilon_{\alpha\beta i} \\ & + i(g_4 - g_3)\sigma_i\hat{k}_i\hat{k}_j\epsilon_{\alpha\beta j}, \end{aligned} \tag{A7}$$

where σ_i ($i = x, y, z$) are the Pauli spin matrices acting on the spin states of the antiproton, $\epsilon_{\alpha\beta\gamma}$ is the fully antisymmetric tensor, $\hat{k}_\alpha$ are the Cartesian components of a unit vector $\hat{\mathbf{k}}$ pointing along the beam momentum, and g_i ($i = 1, \ldots, 4$) are complex amplitudes. When considering Eqs. (A1) and (A7) together, one can find that in collinear kinematics with $OZ||\hat{\mathbf{k}}$: $A_2 = A_4 = A_6 = A_8 = A_9 = A_{12} = 0, A_3 = A_5, A_{10} = A_{11}$. The independent amplitudes g_i are related with the amplitudes A_i via

$$\begin{aligned} & g_1 = A_1 + A_3, \quad g_2 = A_1 + A_3 + A_5, \\ & g_3 = -A_{10}, \quad g_4 = -A_7. \end{aligned} \tag{A8}$$

Taking into account the proper normalization of the scattering matrix $M_{\bar{p}d}$ and using those relations between the A_i's and g_i's, the total hadronic cross sections in Eq. (11) given in Ref. [8] on the basis of the generalized optical theorem can be rewritten as

$$\begin{aligned} & \sigma_0 = \frac{4}{3}\sqrt{\pi}\,\mathrm{Im}(2g_1 + g_2), \quad \sigma_1 = -4\sqrt{\pi}\,\mathrm{Im}(g_3)\,, \\ & \sigma_2 = -4\sqrt{\pi}\,\mathrm{Im}(g_4 - g_3), \quad \sigma_3 = 4\sqrt{\pi}\,\mathrm{Im}(g_1 - g_2). \end{aligned} \tag{A9}$$

Please note that the expressions for the σ_i presented in Eqs. (19)–(20) of our previous work [8] are erroneous. Specifically, the correct signs of σ_1 and σ_2 are opposite to those given in Ref. [8]. Numerically those errors have practically no influence on the value of σ_0 and also not on the absolute values of the polarization efficiencies in the considered energy region of 50–300 MeV, as we verified in corresponding computations.

[1] V. Barone *et al.* (PAX Collaboration), arXiv:hep-ex/0505054.
[2] F. Rathmann *et al.*, Phys. Rev. Lett. **94**, 014801 (2005).
[3] F. Rathmann *et al.*, Phys. Rev. Lett. **71**, 1379 (1993).
[4] W. Augustyniak *et al.*, Phys. Lett. B **718**, 64 (2012).
[5] A. I. Milstein and V. M. Strakhovenko, Phys. Rev. E **72**, 066503 (2005).
[6] P. Lenisa and F. Rathmann (PAX Collaboration), arXiv:nucl-ex/0512021.
[7] C. Barschel *et al.* (PAX Collaboration), arXiv:0904.2325.
[8] Yu. N. Uzikov and J. Haidenbauer, Phys. Rev. C **79**, 024617 (2009).
[9] T. Hippchen, J. Haidenbauer, K. Holinde, and V. Mull, Phys. Rev. C **44**, 1323 (1991).
[10] V. Mull, J. Haidenbauer, T. Hippchen, and K. Holinde, Phys. Rev. C **44**, 1337 (1991).
[11] V. Mull and K. Holinde, Phys. Rev. C **51**, 2360 (1995).
[12] J. Haidenbauer, J. Phys. Conf. Ser. **295**, 012094 (2011).
[13] S. G. Salnikov, Nucl. Phys. A **874**, 98 (2012).
[14] R. Timmermans, T. A. Rijken, and J. J. de Swart, Phys. Rev. C **50**, 48 (1994).
[15] D. Zhou and R. G. E. Timmermans, Phys. Rev. C **86**, 044003 (2012).
[16] R. J. Glauber, *Lectures in Theoretical Physics* (Interscience, New York, 1959), p. 315.
[17] A. G. Sitenko, Ukr. Fiz. Zh. **4**, 152 (1959).
[18] V. Franco and R. Glauber, Phys. Rev. **142**, 1195 (1966).
[19] D. R. Harrington, Phys. Rev. **184**, 1745 (1969).
[20] T. A. Osborn, Ann. Phys. (NY) **58**, 417 (1970).
[21] V. M. Kolybasov and L. A. Kondratyuk, Yad. Fiz. **18**, 316 (1973).
[22] A. Bianconi and M. Radici, Phys. Rev. C **53**, R563 (1996).
[23] R. Crespo, E. Cravo, A. Deltuva, M. Rodriguez-Gallardo, and A. C. Fonseca, Phys. Rev. C **76**, 014620 (2007).
[24] B. Van Overmeire and J. Ryckebusch, Phys. Lett. B **650**, 337 (2007).
[25] Ch. Elster, T. Lin, W. Glöckle, and S. Jeschonnek, Phys. Rev. C **78**, 034002 (2008).
[26] L. A. Kondratyuk, M. Shmatikov, and R. Bizzari, Yad. Fiz. **33**, 795 (1981).
[27] J. Mahalanabis, Nucl. Phys. B Proc. Suppl. **8**, 268 (1989).
[28] M. N. Platonova and V. I. Kukulin, Phys. Rev. C **81**, 014004 (2010).
[29] M. N. Platonova and V. I. Kukulin, Phys. Atom. Nucl. **73**, 86 (2010) [Yad. Fiz. **73**, 90 (2010)].
[30] J. Haidenbauer and Yu. N. Uzikov, in Proceedings of the International meeting on Spin Research Programme, SPIN-Praha-2012, Prague, Czech Republic, July 1–8, 2012 (unpublished), arXiv:1212.2761.
[31] R. J. Glauber and V. Franco, Phys. Rev. **156**, 1685 (1967).
[32] Zhang Yu-Shun and B. A. Robson, Eur. Phys. J. A **22**, 515 (2004).
[33] Yu. N. Uzikov, J. Haidenbauer, and B. A. Prmantayeva, Phys. Rev. C **84**, 054011 (2011).
[34] G. Bruge *et al.*, Phys. Rev. C **37**, 1345 (1988).
[35] R. Machleidt, Phys. Rev. C **63**, 024001 (2001).
[36] M. Lacombe, B. Loiseau, R. Vinh Mau, J. Côté, P. Pirés, and R. de Tourreil, Phys. Lett. B **101**, 139 (1981).
[37] R. Bizzarri *et al.*, Nuovo Cimento A **22**, 225 (1974).
[38] T. Kalogeropoulos and G. S. Tzanakos, Phys. Rev. D **22**, 2585 (1980).
[39] R. D. Burrows *et al.*, Aust. J. Phys. **23**, 919 (1970).
[40] A. S. Carroll *et al.*, Phys. Rev. Lett. **32**, 247 (1974).
[41] R. P. Hamilton, T. P. Pun, R. D. Tripp, D. M. Lazarus, and H. Nicholson, Phys. Rev. Lett. **44**, 1182 (1980).
[42] N. N. Nikolaev and F. Pavlov, in *Proceedings of the 17th International Spin Physics Symposium, Kyoto, October 2006*, edited K. Imai, T. Murakami, N. Saito, and K. Tanida (AIP, New York, 2007) [AIP Conf. Proc. **915**, 932 (2007)].
[43] V. F. Dmitriev, A. Milstein, and S. Salnikov, Phys. Lett. B **690**, 427 (2010).
[44] Yu. N. Uzikov, J. Haidenbauer, J. Phys.: Conf. Ser. **295**, 012087 (2011).
[45] B. Wojtsekhowski, J. Phys. Conf. Ser. **295**, 012128 (2011).
[46] M. P. Rekalo, N. M. Piskunov, and I. M. Sitnik, Few-Body Syst. **23**, 187 (1998).
[47] Yu. N. Uzikov, Phys. Elem. Chast. At. Yadr. **29**, 1405 (1998); Phys. Part. Nucl. **29**, 583 (1998).